ELSEVIER

Journal of Nuclear Materials 240 (1997) 144–153

journal of nuclear materials

Experimental validation of radioactivity calculation for candidate fusion materials

A. Kumar [a,*], Y. Ikeda [b], M.A. Abdou [a]

[a] *School of Engineering and Applied Science, University of California (UCLA), Los Angeles, CA 90095, USA*
[b] *Department of Reactor Engineering, Japan Atomic Energy Research Institute, Tokai, Ibaraki 319-11, Japan*

Received 11 October 1995; accepted 30 August 1996

Abstract

Experiments to measure radioactivity were carried out within the framework of the USDOE/JAERI collaborative program on fusion neutronics. High purity samples of a large number of materials of interest to designers were irradiated at various locations inside a number of prototypical assemblies driven by D–T neutrons. The isotopic activity of γ-emitting radioactive products was then measured and compared to calculations done using activation cross-section libraries of leading radioactivity codes like ACT4, DKR-ICF, RACC and REAC-3. Comparison of calculation C to experiment E of isotopic activities of the irradiated materials shows large variation in C/E ratios for most of the measured isotopic activities. A theoretical approach is outlined to obtain C/E for decay heat for elements and alloys from C/E's of measured isotopic activities of the elemental components. The application of this approach is then demonstrated by obtaining C/E's for PCA, V–15Cr–5Ti, HT-9, modified HT-9 and eight elemental components comprising titanium, vanadium, chromium, manganese, iron, cobalt, nickel, and molybdenum.

1. Introduction

Decay heat in a deuterium–tritium (D–T) fusion reactor environment results from de-excitation of neutron-induced radioactive isotopes via beta decay (electron/positron emission), isomeric transition (IT), or electron capture (EC). Almost invariably, beta decay and electron capture are accompanied by gamma decay. Thus measurement of gamma spectra emitted by the radioactive isotopes is capable of providing invaluable, experimental information on a predominant component of their decay heat. This information can be utilized to validate activation cross-section data libraries used by radioactivity codes.

A series of experimental measurements of D–T neutron induced radioactivity were carried out in samples of various materials in the framework of the USDOE/JAERI collaborative program. Different neutron energy spectra were produced and utilized during different phases of this experimental program. The isotopic activities were measured via gamma spectroscopy of the irradiated samples. The experiments (E) were then compared to calculations (C) that employed activation cross-section libraries of major radioactivity codes. Significant deviations in C/E ratios have been observed for most of the isotopic activities. These experiments and calculations are reviewed in the following sections. It needs to be emphasized that neutron fluences available in these experiments did not permit us to investigate the impact of impurities in the production of induced radioactivity. At least two orders increase in neutron fluence will be needed to see the impact of impurities. At present, such a large amount of D–T neutron fluence is not available anywhere in the world.

A theoretical approach is proposed to obtain C/E ratio for decay heat from C/E's of constituent isotopic activities. Applications of this approach to elemental and alloy materials are demonstrated for a relatively soft neutron energy spectrum.

* Corresponding author. 43-133, E4, 405 Hilgard Avenue, University of California, Los Angeles, CA 90095-1597, USA. Tel.: +1-310 825 8627; fax: +1-310 825 2599; e-mail: kumar@fusion.ucla.edu.

SSDI 0022-3115(96)00489-8

2. Experiments

Elaborate experimental assemblies were constructed to simulate prototypical fusion neutron spectra under the USDOE/JAERI collaborative program [1–4]. The experiments were conducted jointly at the fusion neutronics source facility of the Japanese Atomic Energy Research Institute. Two accelerator based D–T neutron sources, with nominal intensities of 5×10^{12} and 5×10^{11} n/s, were utilized. In addition to a conventional, stationary point neutron source, a line source was experimentally simulated by periodic, linear, relative motion of assembly/detectors with respect to a stationary point neutron source. The latter source distribution simulated more realistically the spatial distribution of a fusion reactor neutron source. In each experimental assembly, sets of material samples were located at two to three locations to cover different neutron energy spectra. A typical sample, say, a foil, was a circular disc measuring 10 mm diameter by 1 mm thickness. Only high purity foils were procured for the experiments. Fig. 1 is a schematic view of an experimental arrangement used during phase IIC of the program. Position A, at 100 mm distance from the neutron source on the target, simulates a hard neutron energy spectrum. Position B, at a distance of 820 mm from the target and inside lithium oxide test section, simulates a relatively soft neutron energy spectrum that could be taken as prototypical of the first wall neutron energy spectrum in a fusion reactor.

The materials irradiated during the entire program included magnesium, aluminum, silicon, titanium, vanadium, chromium, iron, manganese, cobalt, nickel, type 316 stainless steel, copper, zinc, zirconium, niobium, molybdenum, silver, indium, tin, europium 151 (97.7%), europium 153 (99.2%), terbium, dysprosium, holmium, hafnium, tantalum, tungsten, rhenium, iridium, gold, and lead. The D–T neutron fluence ranged from $\sim 10^{10}$ to $\sim 1.7 \times 10^{15}$ n/cm^2. Intrinsic germanium detectors, with high resolution, were deployed for γ-spectroscopy of the irradiated samples, following cooling times ranging from minutes to weeks for short half life ($< \sim 1$ year) isotopes, and for a year or more for longer half life isotopes.

Count spectra for various irradiation times, cooling times, and neutron energy spectra for each material sample were processed to obtain isotopic activities and associated experimental errors [1–4]. An isotopic activity represents the number of emitted γ-rays of a specific energy from a radioactive product of an irradiated material. Tabular data on isotopic activities, available in Kumar et al. [4], were normalized to 1 g of the irradiated material and source neutron strength of 10^{12} n/s. In all, the data for fourteen spectral locations were processed to generate isotopic activities for short half life products. Experimental error is a complex function of numerous parameters and varied from $\sim 1\%$ to $\sim 10\%$ for the great majority of the isotopic activities. Fig. 2 compares decay gamma-ray emission rates per gram of the irradiated material as a function of its Z, charge number. The experimental data, pertaining to phase IIC of the program, has been extrapolated to the same cooling time of one day. Further, the data is normalized to the same D–T neutron fluence. Associated experimental error is also shown. One can observe the following:

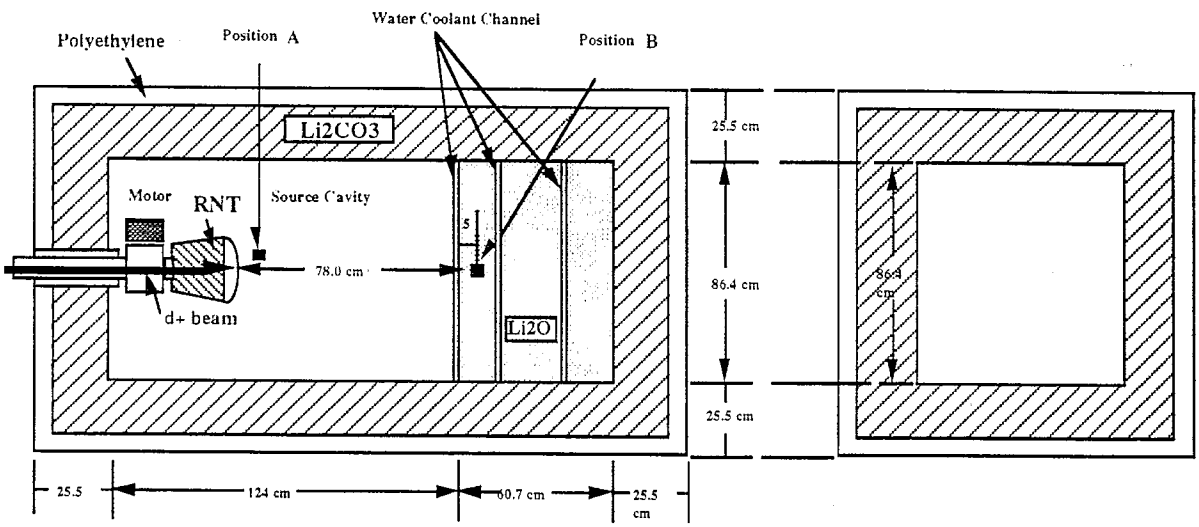

Fig. 1. Typical arrangement of sample materials in phase IIC of USDOE/JAERI collaborative experiments.

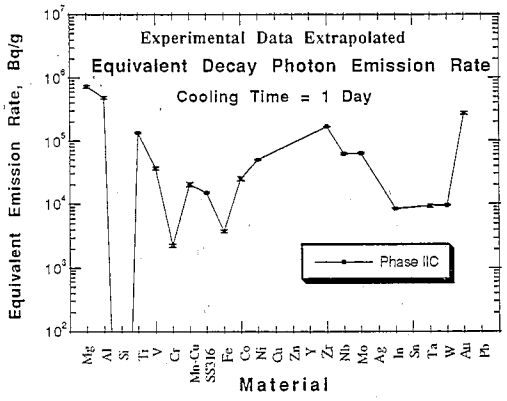

Fig. 2. Gamma emission rate/g versus Z (charge number) of a sample for ~ 1 day cooling time.

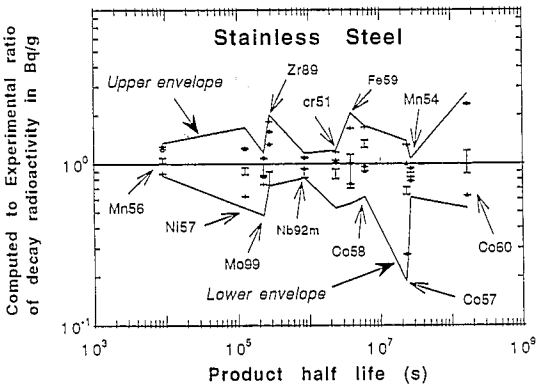

Fig. 4. Type 316 stainless steel: C/E (calculation to experiment) dispersion, for isotopic activities expressed in Bq/g, with ACT4, DKR-ICF, RACC, and REAC-3 activation cross-section libraries.

(i) titanium gives out many more γ-rays than even molybdenum or nickel, (ii) vanadium has more activity than iron.

3. Predictability of isotopic activity

Calculation of an experimentally measured isotopic activity involves the neutron energy spectrum, irradiation time, cooling time, isotopic half life, γ-ray branching ratio, level transitions, decay modes and activation cross-section data, among others. The detailed procedure for calculation of isotopic activity as well as associated uncertainty has been elaborated by Kumar and Ikeda [3]. The neutron energy spectra for various experimental locations were obtained through neutron transport calculations with three-dimensional Monte Carlo code MCNP [5], and two-dimensional discrete ordinates' code system DORT [6]. The cross-section data libraries were based on ENDF/B-V and were processed by MacFarlane [7]. Fig. 3 compares neutron energy spectra, in units of n/cm^2/unit lethargy

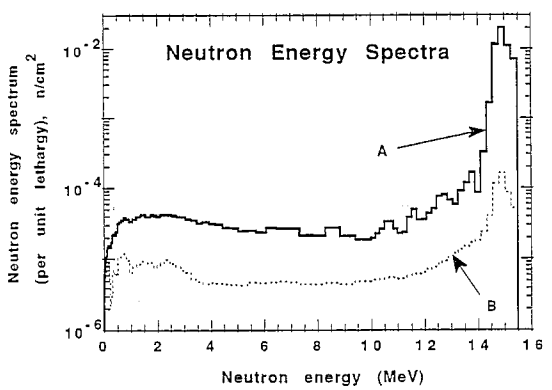

Fig. 3. Computed neutron energy spectra per unit lethargy (n/cm^2) as a function of neutron energy for spatial locations A and B in phase IIC experimental assembly.

for one D–T source neutron, for the locations A and B of the phase IIC experimental assembly. Note that whereas the high energy peak for location B at ~ 14 MeV drops by 2 orders of magnitude with respect to that for location A, the drop in the neutron energy spectrum below this peak is much lower. For example, at 2 MeV, the neutron spectrum is only a factor of ~ 4 lower for the location B. Obviously, the neutron spectrum is significantly softer for location B.

The isotopic half lives, γ-ray branching ratios, decay modes and level transition data were adopted from Browne and Firestone [8]. As for activation cross-section data, libraries accompanying four leading radioactivity codes, e.g., ACT4 [9], DKR-ICF [10], RACC [11], and REAC-3 [12], were adopted. In addition, ENDF/B-VI and JENDL-3 cross-section data were also deployed whenever available [1–3].

The calculated isotopic activities were compared to the experimental data to obtain C/E ratios for each of the activation cross-section library. We notice large deviations between calculation and experiment for almost all the materials. Also, there is relatively large disagreement among the calculations themselves — due to differences in activation cross-section data for the same isotopic activity [1–3]. As an illustrative example, refer to Fig. 4 that shows C/E dispersion for isotopic activities observed for a type 316 stainless steel sample irradiated under different neutron energy spectra. The maximal D–T neutron fluence in the experiments for this material was $\sim 3 \times 10^{13}$ n/cm^2, with irradiation time not exceeding 10 h. The figure shows upper and lower envelope lines. An envelope line was obtained by joining the highest (for upper envelope) or the lowest (for lower envelope) C/E values for each product [1]. For each product, an activation cross-section library and neutron energy spectrum constitute as variables for these plots. One can observe relatively large C/E dispersions for ^{60}Co (half life = 5.3 year), ^{57}Co, ^{58}Co, ^{59}Fe,

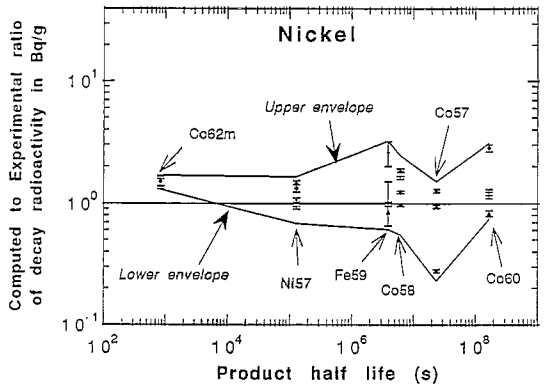

Fig. 5. Nickel C/E (calculation to experiment) dispersion, for isotopic activities expressed in Bq/g, with ACT4, DKR-ICF, RACC, and REAC-3 activation cross-section libraries.

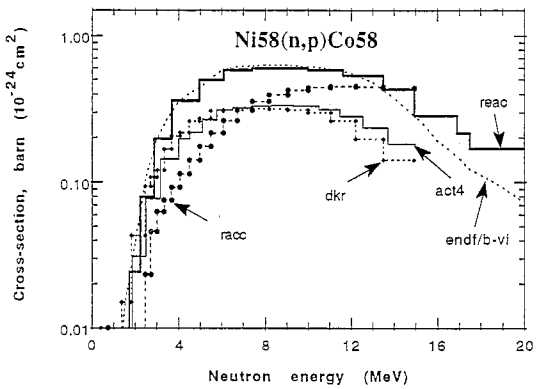

Fig. 7. Cross-section, in barn (10^{-24} cm^2), as a function of neutron energy (MeV) for ^{58}Ni(n, p)^{58}Co activation reaction as represented in ACT4, DKR-ICF, RACC, and REAC-3 activation cross-section libraries.

^{99}Mo, ^{89}Zr, and ^{57}Ni (half life = 36 h). For 100% pure samples of nickel and cobalt, the comprehensive trends of C/E ratios are captured in Figs. 5 and 6, respectively. One can understand by looking at Fig. 5 for nickel, how a discrepancy in prediction of a nickel product, say, ^{57}Co, carries itself into the corresponding discrepancy for SS316 that has nickel as one of its important constituents. Remark from Figs. 5 and 6 that deviations in C/E from 1 are considerable for longer half life products for both nickel and cobalt. An important underlying reason of deviation of C/E lies in the activation cross-section data included in the data libraries used. Figs. 7 and 8 respectively compare activation cross-section representations for ^{58}Ni(n,p)^{58}Co and ^{59}Co(n,γ)^{60}Co reactions as a function of neutron energy. The cross-sections from different data libraries for ^{58}Ni(n,p)^{58}Co reaction differ by as much as a factor of ~ 5 in the energy range displayed in Fig. 7. The cross-section data for ^{59}Co(n,γ)^{60}Co reaction differ by a much larger factor — by three orders of magnitude (see Fig. 8). Viewed against such a large deviation in activation cross-sections for ^{59}Co(n,γ)^{60}Co reaction, the amount of deviation seen in C/E of ^{60}Co in Fig. 6 is fortuitously small!

The inadequacies in modeling of the experimental configuration, transport cross-sections, and methodology of transport solver, activation cross-sections, decay data, and experimental error are among the factors responsible for the C/E dispersion observed for the isotopic activities. It might be almost impossible to eliminate all these contributing factors unless one is willing to invest stupendous efforts over a long time. However, it is possible to target major discrepancies and mitigate them. Also, one can look at an ensemble of C/E's from each of the activation cross-section libraries to qualitatively evaluate them for their respective performances. Fig. 9 is a plot of probability density distribution of C/E's as a function of C/E for each of the four libraries, e.g., ACT4, DKR-ICF, RACC, and REAC-3 [1]. Note that this plot embraces a large numbers of materials, irradiation times, and neutron energy

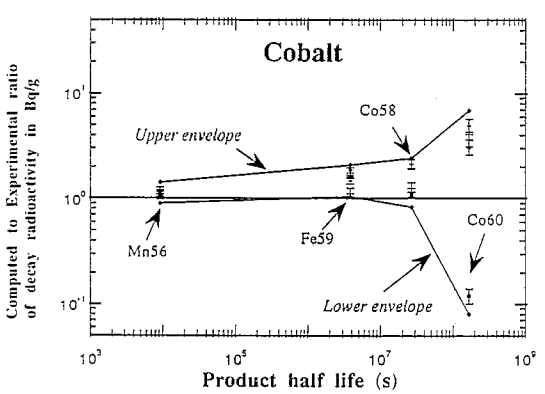

Fig. 6. Cobalt C/E (calculation to experiment) dispersion, for isotopic activities expressed in Bq/g, with ACT4, DKR-ICF, RACC, and REAC-3 activation cross-section libraries.

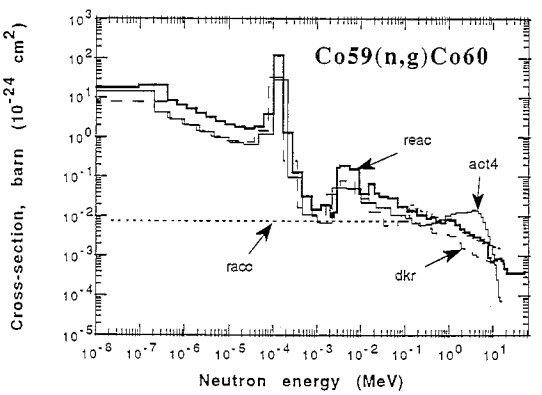

Fig. 8. Cross-section, in barn (10^{-24} cm^2), as a function of neutron energy (MeV) for ^{59}Co(n, γ)^{60}Co activation reaction as represented in ACT4, DKR-ICF, RACC, and REAC-3 activation cross-section libraries.

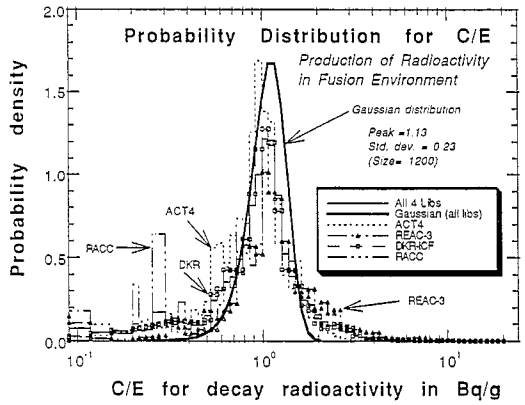

Fig. 9. Probability density distributions of C/E's, for isotopic activities in Bq/g, with ACT4, DKR-ICF, RACC, and REAC-3 activation cross-section libraries.

spectra in our wide ranging experimental effort, as described in the introductory section [1]. Ideally, one would expect this distribution to be a delta function centered at C/E = 1.0. However, the plotted distributions extend from very low C/E's to quite large C/E's. Fig. 9 also shows a consolidated probability density distribution, covering all the four libraries, as well as a corresponding Gaussian distribution. Note that the Gaussian distribution peaks at C/E = 1.13. This implies that the libraries, as a whole, have a tendency to overpredict an average isotopic activity.

4. A theoretical approach for prediction of decay heat

As for predictability, i.e., C/E, of decay heat from radioactive isotopes of an irradiated material is concerned, one can directly use C/E for the corresponding isotopic activity, as discussed in the preceding section. However, from a reactor designer standpoint, one would rather be interested in determining predictability of sum decay heat from all contributing isotopic activities for any irradiated material. In principle, it is possible to make use of C/E data for individual isotopic activities to predict C/E of decay heat for a material. We outline a theoretical approach below.

Let us imagine a composite material consisting of NE elements. An elemental component m has a weight fraction of w_m. An element component m generates NI(m) radioactive isotopes when exposed to neutron irradiation. Let $c_{m,i,j}$ stand for calculated decay heat for the ith component of the mth element using the jth library. Also, $e_{m,i}$ represents experimental decay heat for the ith component of the mth element. Then, $(C/E)_j$, the predictability of the net decay heat for the composite material for library j is given by

$$\left(\frac{C}{E}\right)_j = \frac{\sum_{m=1}^{NE} w_m \left(\sum_{i=1}^{NI(m)} c_{m,i,j} \right)}{\sum_{m=1}^{NE} w_m \left(\sum_{i=1}^{NI(m)} c_{m,i,j} \left(\frac{c_{m,i,j}}{e_{m,i}} \right)^{-1} \right)}, \tag{1}$$

where $c_{m,i,j}/e_{m,i}$ is the ratio of calculation to experiment for isotopic activity i of material m for library j, and is already known.

The relative standard deviation on $(C/E)_j$, say, σ_j, is given as

$$\sigma_j = \frac{\sqrt{\sum_{m=1}^{NE} w_m^2 \left[\sum_{i=1}^{NI(m)} c_{m,i,j}^2 \left(c_{m,i,j}/e_{m,i} \right)^{-2} \sigma_{m,i,j}^2 \right]}}{\sum_{m=1}^{NE} w_m \left(\sum_{i=1}^{NI(m)} c_{m,i,j} \right)}, \tag{2}$$

where $\sigma_{m,i,j}$ is the relative standard deviation on $c_{m,i,j}/e_{m,i}$, and is already known. Note that derivation of Eq. (2) from Eq. (1) assumes that there is no correlation among predictability of individual isotopic activities, on one hand, and elemental composition, on the other. Evidently, use of the above formulas is subject to extreme caution for large neutron fluences that lead to significant burn-up and, hence, change in elemental composition. This change will also lead to change in the neutron energy spectrum, and, hence, predictability of isotopic activities. This means that c factors appearing in Eqs. (1) and (2) will have to be modified appropriately in the event of appreciable burn-up of the medium.

The role of the neutron energy spectrum, irradiation time, burn-up of elemental components on the inventory of

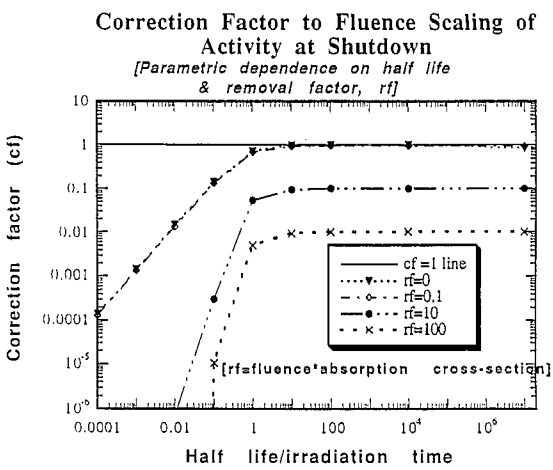

Fig. 10. Correction factor, cf, as a function of neutron fluence, isotopic half life and irradiation time.

isotopic inventory and attendant afterheat (c factors appearing in Eqs. (1) and (2) above) can be studied comprehensively using sophisticated computer codes. However, it is very helpful to use simpler formulations for understanding the interplay of these factors. The activity of radioactive product 'p' of a target isotope 't', say, A_p, can be expressed as

$$A_p = n_t^0 \langle \sigma_{t\to p} \rangle F\lambda \times \left[\frac{\exp(-\langle \sigma_{ta} \rangle F) - \exp(-\lambda t_r)\exp(-\langle \sigma_{pa} \rangle F)}{\lambda t_r + \langle \sigma_{pa} \rangle F - \langle \sigma_{ta} \rangle F} \right], \quad (3)$$

where various terms are defined as below:

A_p product activity in Bq/g;
n_t^0 initial number of target isotopes per g;
$\langle \sigma_{t\to p} \rangle$ effective microscopic reaction cross-section leading to generation of product 'p' from target nucleus 't';
$\langle \sigma_{ta} \rangle$ effective microscopic reaction cross-section of destruction of target;
$\langle \sigma_{pa} \rangle$ effective microscopic reaction cross-section of destruction of product;
λ decay constant of the product;
$F = \Phi t_r$ neutron fluence;
Φ energy integrated neutron flux;
t_r irradiation time.

If neutron reactions with the product nuclei are ignored, Eq. (3) can be simplified to

$$A_p = n_t^0 \langle \sigma_{t\to p} \rangle F\lambda \mathrm{cf}, \quad (4)$$

where cf is called a correction factor, and is given by

$$\mathrm{cf} = \left[\frac{\exp(-\mathrm{rf}) - \exp(-\lambda t_r)}{\lambda t_r - \mathrm{rf}} \right]. \quad (5a)$$

rf stands for removal factor and is defined by

$$\mathrm{rf} = \langle \sigma_{ta} \rangle F. \quad (5b)$$

Fig. 10 shows the correction factor, cf, as a function of product half expressed in units of irradiation time. The

Table 1
Reactions relevant to the analysis of the experimental decay radioactivity data for titanium, vanadium, chromium, manganese, iron, cobalt, nickel

Material	Radioactive isotope (product)	Contributing reactions
Titanium	^{51}Ti	^{50}Ti(n, γ)^{51}Ti
	^{45}Ti	^{46}Ti(n, 2n)^{45}Ti
	^{44}Sc	^{46}Ti(n, t)^{44}Sc
	^{48}Sc	^{48}Ti(n, p)^{48}Sc
		^{49}Ti(n, np)^{48}Sc
		^{49}Ti(n, d)^{48}Sc
		^{50}Ti(n, t)^{48}Sc
	^{47}Sc	^{47}Ti(n, p)^{47}Sc
		^{48}Ti(n, np)^{47}Sc
		^{48}Ti(n, d)^{47}Sc
		^{49}Ti(n, t)^{47}Sc
	^{47}Ca	^{50}Ti(n, α)^{47}Ca
	^{46}Sc	^{46}Ti(n, p)^{46}Sc
		^{47}Ti(n, np)^{46}Sc
		^{47}Ti(n, d)^{46}Sc
		^{48}Ti(n, t)^{46}Sc
Vanadium	^{52}V	^{51}V(n, γ)^{52}V
	^{51}Ti	^{51}V(n, p)^{51}Ti
	^{48}Sc	^{51}V(n, α)^{48}Sc
	^{47}Sc@	^{50}V(n, α)^{47}Sc
		^{51}V(n, n′α)^{47}Sc
Chromium	^{49}Cr	^{50}Cr(n, 2n)^{49}Cr
	^{51}Cr	^{52}Cr(n, 2n)^{51}Cr
		^{50}Cr(n, γ)^{51}Cr
Manganese	^{52}V	
	^{56}Mn	^{55}Mn(n, α)^{52}V
	^{54}Mn	^{55}Mn(n, γ)^{56}Mn
		^{55}Mn(n, 2n)^{54}Mn
Iron	^{53}Fe	^{54}Fe(n, 2n)^{53}Fe
	^{56}Mn	^{56}Fe(n, p)^{56}Mn
		^{57}Fe(n, np)^{56}Mn
		^{57}Fe(n, d)^{56}Mn
		^{58}Fe(n, t)^{56}Mn
	^{51}Cr	^{54}Fe(n, α)^{51}Cr
	^{59}Fe	^{58}Fe(n, γ)^{59}Fe
	^{54}Mn	^{54}Fe(n, p)^{54}Mn
Cobalt	^{56}Mn	^{59}Co(n, α)^{56}Mn
	^{59}Fe	^{59}Co(n, p)^{59}Fe
	^{58}Co	^{59}Co(n, 2n)^{58}Co
		^{59}Co(n, 2n)^{58m}Co → ^{58}Co
	^{60}Co	^{59}Co(n, γ)^{60}Co
		^{59}Co(n, γ)^{60m}Co → ^{60}Co
Nickel	^{62m}Co	^{62}Ni(n, p)^{62m}Co
	^{65}Ni	^{64}Ni(n, γ)^{65}Ni
	^{57}Ni	^{58}Ni(n, 2n)^{57}Ni
	^{59}Fe	^{62}Ni(n, α)^{59}Fe
		^{60}Ni(n, 2p)^{59}Fe
	^{58}Co	^{58}Ni(n, p)^{58}Co
		^{58}Ni(n, p)^{58m}Co → ^{58}Co
	^{57}Co	^{58}Ni(n, np)^{57}Co
		^{58}Ni(n, d)^{57}Co
		(also ^{57}Ni → ^{57}Co)
	^{60}Co	^{60}Ni(n, p)^{60}Co
		^{61}Ni(n, np)^{60}Co
		^{61}Ni(n, d)^{60}Co
		^{62}Ni(n, t)^{60}Co
		^{60}Ni(n, p)^{60m}Co → ^{60}Co
		^{61}Ni(n, np)^{60m}Co → ^{60}Co
		^{61}Ni(n, d)^{60m}Co → ^{60}Co

Table 2
Reactions relevant to the analysis of the experimental decay radioactivity data for molybdenum

Material	Radioactive isotope (product)	Contributing reactions	Material	Radioactive isotope (product)	Contributing reactions
Molybdenum	^{101}Tc	^{100}Mo(n, γ)^{101}Mo → ^{101}Tc	Molybdenum	^{89}Zr	^{92}Mo(n, α)^{89}Zr
	^{101}Mo	^{100}Mo(n, γ)^{101}Mo			^{92}Mo(n, α)^{89m}Zr → ^{89}Zr
	^{91}Mo	^{92}Mo(n, 2n)^{91}Mo			
		^{92}Mo(n, 2n)^{91m}Mo → ^{91}Mo		^{95m}Nb	^{95}Mo(n, p)^{95m}Nb
	^{98m}Nb	^{98}Mo(n, p)^{98m}Nb			^{96}Mo(n, np)^{95m}Nb
		^{100}Mo(n, t)^{98m}Nb			^{96}Mo(n, d)^{95m}Nb
		^{100}Mo(n, nd)^{98m}Nb			^{97}Mo(n, t)^{95m}Nb
	^{97}Nb	^{97}Mo(n, p)^{97}Nb			^{98}Mo(n, nt)^{95m}Nb
		^{98}Mo(n, np)^{97}Nb			(also ^{95}Zr → ^{95m}Nb)
		^{98}Mo(n, d)^{97}Nb			
		(and ^{97}Zr → ^{97m}Nb → ^{97}Nb)		^{92m}Nb	^{92}Mo(n, p)^{92m}Nb
	^{93m}Mo	^{94}Mo(n, 2n)^{93m}Mo		^{95}Nb	^{95}Mo(n, p)^{95}Nb
		^{92}Mo(n, γ)^{93m}Mo			^{96}Mo(n, np)^{95}Nb
	^{96}Nb	^{96}Mo(n, p)^{96}Nb			^{96}Mo(n, d)^{95}Nb
		^{97}Mo(n, np)^{96}Nb			^{97}Mo(n, t)^{95}Nb
		^{97}Mo(n, d)^{96}Nb			^{98}Mo(n, nt)^{95}Nb
		^{98}Mo(n, t)^{96}Nb			(also ^{95m}Nb → ^{95}Nb)
	^{99}Mo	^{100}Mo(n, 2n)^{99}Mo		^{91}Nb	(^{91}Mo → ^{91}Nb)
		^{98}Mo(n, γ)^{99}Mo		^{95}Zr	^{98}Mo(n, α)^{95}Zr
				^{88}Zr	^{92}Mo(n, nα)^{88}Zr

removal factor, rf, is varied from 0 to 100. Note that, for longer half life products — half life/irradiation time ratio significantly exceeding unity — cf stays close to unity as long as rf is ~0.1 or less. As rf rises, cf decreases almost as 1/rf. This would then translate into A_p staying almost constant as rf is raised above ~0.1. However, for short half life products, the correction factor cf and activity A_p have non-linear dependence on rf (and F).

5. Discussion on predictability of decay heat

The approach described in the preceding section has been applied to eight elements, viz. titanium, vanadium, chromium, manganese, iron, cobalt, nickel, and molybdenum. For each element, we have calculated C/E's for three modes of decay heat: (i) total decay heat, which

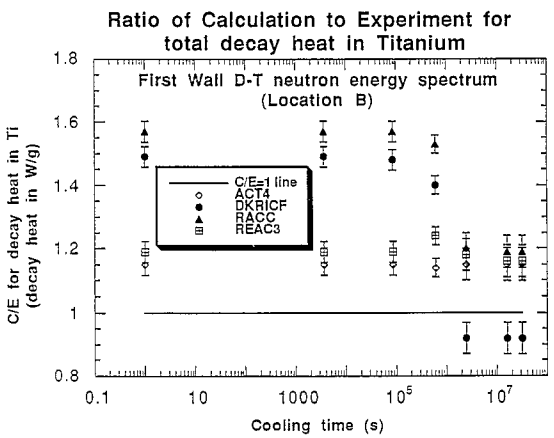

Fig. 11. Total decay heat (W/g) in titanium: calculation-to-experiment ratio for ACT4, DKR-ICF, RACC, and REAC-3 libraries, for location B of phase IIC experimental assembly (D–T neutron source intensity of 10^{12} n/s for a total irradiation time of 9 h).

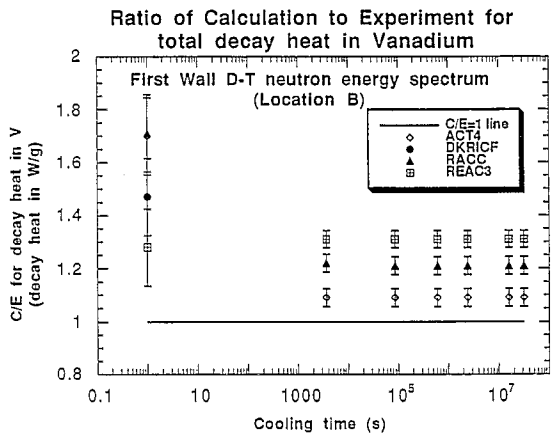

Fig. 12. Total decay heat (W/g) in vanadium: calculation-to-experiment ratio for ACT4, DKR-ICF, RACC, and REAC-3 libraries, for location B of phase IIC experimental assembly (D–T neutron source intensity of 10^{12} n/s for a total irradiation time of 9 h).

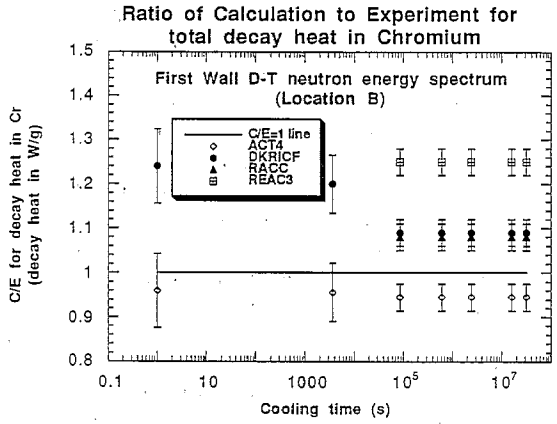

Fig. 13. Total decay heat (W/g) in chromium: calculation-to-experiment ratio for ACT4, DKR-ICF, RACC, and REAC-3 libraries, for location B of phase IIC experimental assembly (D–T neutron source intensity of 10^{12} n/s for a total irradiation time of 9 h).

includes all components like decay γ-rays, electrons and positrons, and internal bremsstrahlung [8], (ii) pure γ-ray decay heat, which includes only decay γ-rays, and (iii) 'no γ-ray' decay heat, which excludes decay γ-rays only. Significant differences have been observed in predictability of these three modes of decay heat. However, in what follows, we will focus only on total decay heat.

Table 1 catalogs the reactions contributing to experimental measurements of the radioactivity in titanium, vanadium, chromium, manganese, iron, cobalt, and nickel. Table 2 provides similar information for molybdenum. For molybdenum alone, there are 38 contributing reaction channels! Due to so many reactions involved, as shown in

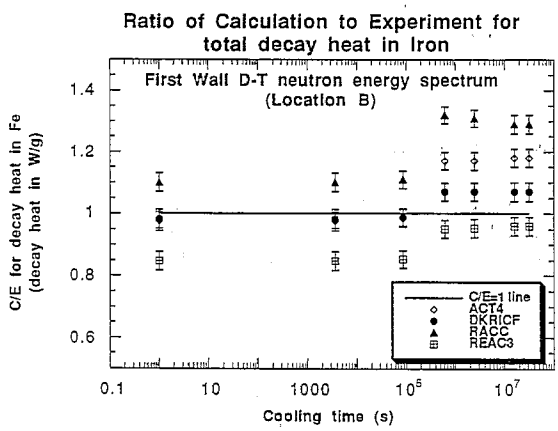

Fig. 14. Total decay heat (W/g) in iron: calculation-to-experiment ratio for ACT4, DKR-ICF, RACC, and REAC-3 libraries, for location B of phase IIC experimental assembly (D–T neutron source intensity of 10^{12} n/s for a total irradiation time of 9 h).

Table 3
Elemental composition of the alloys considered

Elemental component	wt% of elemental components in alloy			
	PCA	V–15Cr–5Ti	HT-9	modified HT-9
Titanium	0.3	5.0	0.0	0.0
Vanadium	0.0	79.8	0.0	0.0
Chromium	14.0	15.0	11.5	11.5
Manganese	1.8	0.0	0.5	0.5
Iron	65.12	0.01	85.24	85.72
Cobalt	0.03	0.0	0.0	0.0
Nickel	16.0	0.001	0.5	0.0025
Molybdenum	2.0	0.008	1.0	0.02

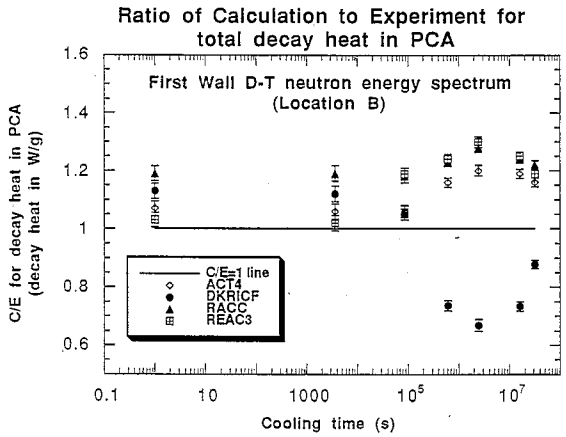

Fig. 15. Total decay heat (W/g) in PCA: calculation-to-experiment ratio for ACT4, DKR-ICF, RACC, and REAC-3 libraries, for location B of phase IIC experimental assembly (D–T neutron source intensity of 10^{12} n/s for a total irradiation time of 9 h).

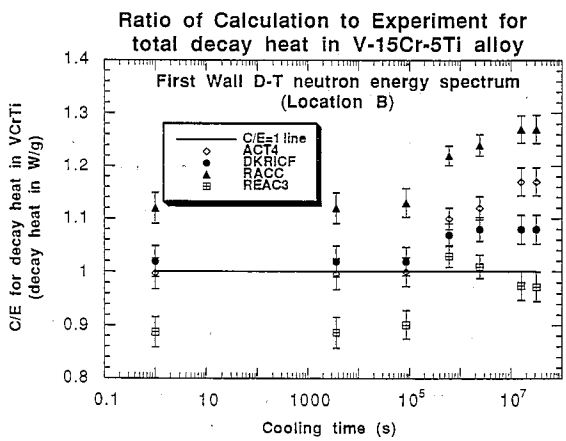

Fig. 16. Total decay heat (W/g) in V–15Cr–5Ti alloy: calculation-to-experiment ratio for ACT4, DKR-ICF, RACC, and REAC-3 libraries, for location B of phase IIC experimental assembly (D–T neutron source intensity of 10^{12} n/s for a total irradiation time of 9 h).

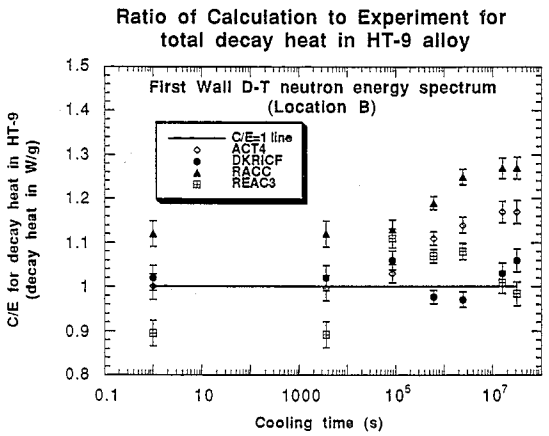

Fig. 17. Total decay heat (W/g) in HT-9: calculation-to-experiment ratio for ACT4, DKR-ICF, RACC, and REAC-3 libraries, for location B of phase IIC experimental assembly [D–T neutron source intensity of 10^{12} n/s for a total irradiation time of 9 h).

these two tables, it is clear that one can readily understand an important role of comparison of calculations to the experiments before approving an activation cross-section data library for continued use in the future.

Figs. 11–14 show C/E ratios of total decay heat as a function of cooling time for titanium, vanadium, chromium, and iron. The decay heat data is for location B of phase IIC. As mentioned earlier, the neutron energy spectrum for this location is prototypical of a first wall spectrum in a fusion reactor. The associated uncertainty for each data point is also included. Note that C/E's lie both above and below the C/E = 1 line for all the four materials except for vanadium, all C/E's for the latter lying systematically above the C/E = 1 line. The irradiation time is 9 h at a

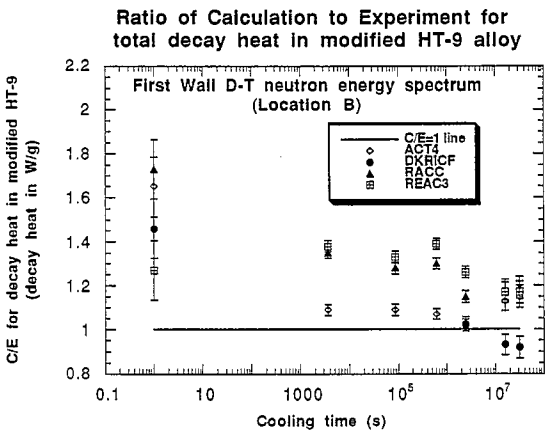

Fig. 18. Total decay heat (W/g) in modified HT-9: calculation-to-experiment ratio for ACT4, DKR-ICF, RACC, and REAC-3 libraries, for location B of phase IIC experimental assembly (D–T neutron source intensity of 10^{12} n/s for a total irradiation time of 9 h).

D–T neutron intensity of 10^{12} n/s. Generally speaking, for a given cooling time, isotopic activities with half lives comparable to this cooling time make relatively significant contributions to the prediction of the total decay heat.

We have also looked at predictability of total decay heat for leading alloys (steels) for fusion reactors. These include PCA, V–15Cr–5Ti, HT-9 and modified HT-9. The elemental compositions for these alloys were adopted from Fetter [13] and are shown in Table 3. The calculations were done for the same spectrum and fluence as used for the elemental materials above. Figs. 15–18 show C/E for total decay heat in PCA, V–15Cr–5Ti, HT-9, and modified HT-9, respectively. Remark a tendency of all the four libraries to overpredict total decay heat, as also observed for the elemental components discussed earlier (see Figs. 11–14).

6. Summary and conclusions

The USDOE/JAERI program of fusion neutron induced radioactivity measurements has provided an invaluable opportunity to obtain prediction uncertainty data for individual isotopic activities generated in materials subjected to irradiation. Activation cross-section libraries of four leading radioactivity codes, e.g., ACT4, DKR-ICF, RACC, and REAC-3, were deployed to calculate C/E ratios for isotopic activities in titanium, vanadium, chromium, manganese, iron, cobalt, nickel, molybdenum, and a host of other materials, for all the fluence and spectral conditions of the experiments. Considerable deviations from unity have been noted for almost all the isotopic activities. A theoretical approach has been described in this paper to obtain prediction uncertainty on total decay heat from component isotopic activities for elemental as well as alloy materials. This approach was applied to obtain C/E trends for decay heat as a function of cooling time for titanium, vanadium, chromium, manganese, iron, cobalt, nickel, molybdenum, on one hand, and for PCA, V–15Cr–5Ti, HT-9, and modified HT-9 alloys, on the other.

Acknowledgements

The US contribution was supported by the United States Department of Energy, Office of Fusion Energy, under contract No. DE-FG03-86ER52123.

References

[1] A. Kumar, Y. Ikeda, M.A. Abdou, M.Z. Youssef, C. Konno, K. Kosako, Y. Oyama, T. Nakamura and H. Maekawa, Fusion Technol. 28 (1995) 99.

[2] Y. Ikeda, A. Kumar, C. Konno, K. Kosako, Y. Oyama, F. Maekawa, H. Maekawa, M.Z. Youssef and M.A. Abdou, Fusion Technol. 28 (1995) 74.

[3] A. Kumar and Y. Ikeda, in: Proc. Int. Conf. on Nuclear Data for Science and Technology, Gatlinburg, TN, USA, May 9–13, 1994 (American Nuclear Society, 1994) p. 883.
[4] A. Kumar, Y. Ikeda, M.A. Abdou, M.Z. Youssef, C. Konno, K. Kosako, Y. Oyama, T. Nakamura and H. Maekawa, Induced Radioactivity Measurements in Fusion Neutron Environment: Joint Report of USDOE/JAERI Collaborative Program on Fusion Neutronics, report No. UCLA-ENG-91-32/UCLA-FNT-53, and JAERI-M-93-018 (Feb. 1993).
[5] J.F. Briesmeister, ed., MCNP – A General Monte Carlo Code for Neutron and Photon Transport: Version 3A, report No. LA-7396-M, Rev. 2 (Sept. 1988), along with MCNP3B newsletter, July 18, 1988, Los Alamos National Laboratory.
[6] W.A. Rhoades and R.L. Childs, DOT-IV Version 4.3: One and Two Dimensional Transport Code Collection, RSIC computer code collection CCC-429 (May 1984).
[7] R.E. MacFarlane, TRANSX-CTR: A Guide for Interfacing MATXS Cross-section Libraries to Nuclear Transport Codes for Fusion Systems Analysis, Los Alamos National Laboratory, Report LA-9863-MS (Feb. 1984).
[8] E. Browne and R.B. Firestone, in: Table of radioactive isotopes, ed. V.S. Shirley (Wiley Interscience, New York, 1986).
[9] Y. Seki et al., THIDA-2: An Advanced Code System for Calculation of Transmutation, Activation, Decay Heat and Dose Rate, RSIC computer code collection, CCC-410 (Apr. 1987).
[10] D.L. Henderson and O. Yasar, A Radioactivity and Dose Rate Calculation Code Package, Vol. 1–2, RISC computer code collection, CCC-323 (Apr. 1987).
[11] J. Jung, Theory and Use of the Radioactivity Code RACC, ANL/FPP/TM-122, Argonne National Laboratory (1979).
[12] F.M. Mann, REAC*2: Users Manual and Code Description, WHC-EP-0282 (Westinghouse Hanford, 1989).
[13] S. Fetter, Fusion Technol. 11 (1987) 400.